Modeling of coronal mass ejections that caused particularly large geomagnetic storms using ENLIL heliosphere cone model

A. Taktakishvili,[1,2,3] A. Pulkkinen,[2,4] P. MacNeice,[2] M. Kuznetsova,[2] M. Hesse,[2] and D. Odstrcil[2,5]

Received 15 November 2010; revised 24 February 2011; accepted 22 March 2011; published 16 June 2011.

[1] In our previous paper we reported the results of modeling of 14 selected well-observed strong halo coronal mass ejection (CME) events using the WSA-ENLIL cone model combination. Cone model input parameters were obtained from white light coronagraph images of the CME events using the analytical method developed by Xie et al. (2004). This work verified that coronagraph input gives reasonably good results for the CME arrival time prediction. In contrast to Taktakishvili et al. (2009), where we started the analysis by looking for clear CME signatures in the data and then proceeded to model the interplanetary consequences at 1 AU, in the present paper we start by generating a list of observed geomagnetic storm events and then work our way back to remote solar observations and carry out the corresponding CME modeling. The approach used in this study is addressing space weather forecasting and operational needs. We analyzed 36 particularly strong geomagnetic storms, then tried to associate them with particular CMEs using SOHO/LASCO catalogue, and finally modeled these CMEs using WSA-ENLIL cone model. Recently, Pulkkinen et al. (2010) developed a novel method for automatic determination of cone model parameters. We employed both analytical and automatic methods to determine cone model input parameters. We examined the CME arrival times and magnitude of impact at 1 AU for both techniques. The results of the simulations are compared with the ACE satellite observations. This comparison demonstrated that WSA-ENLIL model combination with coronagraph input gives reasonably good results for the CME arrival times for this set of "geoeffective" CME events as well.

Citation: Taktakishvili, A., A. Pulkkinen, P. MacNeice, M. Kuznetsova, M. Hesse, and D. Odstrcil (2011), Modeling of coronal mass ejections that caused particularly large geomagnetic storms using ENLIL heliosphere cone model, *Space Weather*, *9*, S06002, doi:10.1029/2010SW000642.

1. Introduction

[2] The most severe geomagnetic storms are caused by coronal mass ejection (CME) events [*Gosling*, 1993]. After a CME reaches the Earth environment it can cause damage to satellites, electrical power transformers, disruption of communications. Clearly, for the space weather prediction it is crucial to know the arrival time of a CME at the Earth accurately.

[3] Scientific models are used for space weather forecasting and for space weather operators' applications. It is important that the operational users, forecasters, model developers and the scientific community are aware of model capabilities and limitations. In this paper we study the performance of the WSA-ENLIL cone model combination in modeling CMEs. The approach used in the presented study is addressing space weather forecasting and operational needs.

[4] There have been extensive observational as well as theoretical studies of CMEs in relation to their space weather implications in the recent decade. *Berdichevsky et al.* [2000] studied interplanetary shock statistical properties and their drivers, including solar transients (i.e., CMEs). *Gopalswamy et al.* [2001] developed an empirical

[1]Goddard Earth Science and Technology Center, University of Maryland Baltimore County, Baltimore, Maryland, USA.
[2]NASA Goddard Space Flight Center, Greenbelt, Maryland, USA.
[3]Abastumany Observatory, Tbilisi, Georgia.
[4]Now at Institute of Astrophysics and Computational Physics, Catholic University of America, Washington, D. C., USA.
[5]Department of Computational and Data Sciences, George Mason University, Fairfax, Virginia, USA.

model predicting 1 AU arrival times of CMEs. The model is based on an effective interplanetary acceleration that CMEs experience as they propagate from Sun to 1 AU and the primary input is the initial plane-of-sky speed of white light CMEs obtained using coronagraphs. The model results are in reasonable agreement with observations for high speed CMEs. *Gopalswamy et al.* [2005] extended their empirical model to the prediction of the arrival times of the interplanetary shocks. *Xie et al.* [2006] improved input to the empirical model of *Gopalswamy et al.* [2005] by using the cone model method to determine the CME radial velocity. Recently *Kim et al.* [2007] evaluated the model using 91 interplanetary shocks at 1 AU examining ACE and WIND satellite data. In a number of papers [*Fry et al.*, 2003; *Oler*, 2004; *Dryer et al.*, 2004; *Smith et al.*, 2005; *McKenna-Lawlor et al.*, 2006], the authors studied the performance of three different CME and shock propagation models, a Shock Time of Arrival model (STOA), an Interplanetary Shock Propagation model (ISPM), and the Hakamada-Akasofu-Fry version 2 model (HAFv2), in forecasting shock arrival times for hundreds of events, including the extreme events of the October–November 2003 "Halloween epoch." The STOA, ISPM and HAFv2 models use initial shock speed derived from metric type II radio observations (together with soft X-ray data and solar image data). HAFv2 is the only one of these three that models the variable background solar wind. In all these modeling studies the average error and root mean square error of the ICME shock arrival times to the Earth was 10 or more hours.

[5] *Odstrcil et al.* [2004, 2005] studied the ICME from the 12 May 1997 solar event using ENLIL MHD heliospheric model with two different coronal inputs. *Wu et al.* [2007] used a hybrid code, combining HAFv2 and 3-D MHD simulation, to study the same event. *Tóth et al.* [2007] performed a Sun-to-thermosphere simulation of the 28–30 October 2003 storm with the Space Weather Modeling Framework (SWMF), and *Lugaz et al.* [2007], also using SWMF studied CME events of 24 November 2000. *Kataoka et al.* [2009] recently used a 3-D MHD simulation with spheromak CME model to reproduce the December 2006 CME event.

[6] In our previous papers [*Taktakishvili et al.*, 2009, 2010] we presented the results of the WSA-ENLIL cone modeling for 14 CME events and compared them to ACE observations and two reference model results. The WSA-ENLIL cone model has three components: (1) Wang-Shelley-Arge model, which computes the solar wind speed and magnetic field at the bounding surface using an empirical relationship [*Arge and Pizzo*, 2000]; (2) cone model for halo CMEs, an analytical [*Xie et al.*, 2004] or automatic [*Pulkkinen et al.*, 2010] method to determine the angular width, propagation orientation and radial velocity of halo CMEs; and (3) the ENLIL heliosphere model, a time-dependent 3-D MHD model of the heliosphere, developed by D. Odstrcil [see, e.g., *Odstrcil and Pizzo*, 1999; *Odstrcil et al.*, 2004].

[7] In this paper the criterium for choosing the events is quite different from the criterium of our previous study [*Taktakishvili et al.*, 2009], which was the availability of clear LASCO/C3 images to enable the best possible determination of cone model parameters using the analytical cone model method of *Xie et al.* [2004]. In the present study we start the analysis by identifying 36 particularly strong geomagnetic storms, then associate these storms with particular CMEs using SOHO/LASCO catalogue (http://cdaw.gsfc.nasa.gov/CME_list), and finally carry out CME modeling using WSA-ENLIL cone model. The description of the selection of the events is given in Section 2.

[8] We employed both analytical and automatic methods to determine cone model input parameters. We examined the CME interplanetary shock arrival time, the magnitude of its impact at 1 AU (minimum magnetopause standoff distance), and the maximum electric field induced by the CME for both techniques. The results of the simulation are compared with the ACE satellite observations. Another important parameter in this regard is the B_z component of the interplanetary magnetic field, but for the moment ENLIL model does not take into account the realistic magnetic field structure of the CME cloud, so we do not consider this subject in this paper.

[9] We used WSA 1.6 and ENLIL 2.5 versions available at the Community Coordinated Modeling Center at NASA/GSFC during this study.

2. Selection of the Geomagnetic Storm Events

[10] The 1 h resolution OMNI data for D_{st} and K_p indices from http://omniweb.gsfc.nasa.gov/ was downloaded for the period of January 1996 to February 2009. The selected time period reflects the SOHO/LASCO data availability. First, all moments of time having K_p index greater or equal to 8 were identified in the OMNI data set. The K_p indices 8 and 9 are characterized as "severe" and "extreme" in NOAA space weather scale for geomagnetic storms, respectively. To identify individual storm events, moments of time with $K_p \geq 8$ that had greater than 12 h separation were selected. Note that the selected separation parameter differentiates the "Halloween storms" of 29–31 October 2003, which were caused by different CMEs. To rank the selected storm events, the minimum Dst index value within ±12 h window around these moments of time were identified. Finally, the identified $K_p \geq 8$ events separated by more than 12 h were ranked as a function of the minimum D_{st} index taken over individual events. Table 1 shows the identified 36 events that served as a starting point for our analysis. Here we should also note that not all very strong magnetic storms have large negative D_{st}, the event of 4 August 1972 being classic case in point [*Anderson et al.*, 1974].

3. Brief Description: WSA-ENLIL Cone Model, Analytical and Automatic Methods for the Cone Parameter Determination

[11] *Zhao et al.* [2002] advanced the cone model approximation to determine CME geometric and kinematic

Table 1. The List of the 36 Particularly Strong Geomagnetic Storms Ranked by Minimum D_{st} Index and Corresponding CME Events Studied[a]

Rank	Storm Minimum Dst Time	CME Start Time	Min Dst (nT)	CME Cone Axis Lat. (deg)		CME Cone Axis Lon. (deg)		CME Cone Radius (deg)		CME Vrad (km/s)		Shock Arrival Time Error (h)			
				Analyt.	Auto	Analyt.	Auto	Analyt.	Auto	Analyt.	Auto	Analyt.	Auto	Ref	ESA
01	03-11-20 21	03-11-18 08:50	–422	–18	–11	16	3	50	32	1215	1316	–1	4	2	–21
02[b]	01-03-31 09	01-03-29 10:26	–387	–31	0	–13	0	85	26	913	1267	7	7	11	16
03[b]	03-10-30 23	03-10-29 20:54	–383	19	–4	30	2	85	30	1872	2222	6	11	29	1
04	04-11-08 07	04-11-06 02:06	–373	12	3	–39	–1	85	11	1525	2782	–7	–4	8	1
05[b]	03-10-30 01	03-10-28 11:30	–353	7	0	28	0	83	30	2868	2557	1	10	29	–3
06	00-07-16 01	01-07-14 10:54	–301	22	3	25	4	61	30	1686	1940	6	9	21	–2
07	01-11-06 07	01-11-04 16:35	–292	30	–2	30	3	70	30	1999	2322	–9	–7	16	–9
08	*04-11-10 10*	*multiple CMEs*	*–289*												
09	00-04-07 01	00-04-04 16:32	–288	14	1	27	7	52	31	2038	1626	–15	–6	1	–11
10	01-04-12 00	01-04-10 05:30	–271	–30	–10	26	3	76	28	1260	1773	8	13	16	–15
11	*05-05-15 09*	*NA*	*–263*												
12	*99-10-22 07*	*NA*	*–237*												
13[b]	00-08-12 10	00-08-09 16:30	–235	12	8	25	–2	55	30	960	654	4	20	–1	1
14	01-11-24 17	01-11-22 23:30	–221	–15	4	38	14	71	54	2809	1207	–8	15	17	–2
15	*05-08-24 12*	*multiple CMEs*	*–216*												
16	*98-09-25 10*	*no image*	*–207*												
17	98-05-04 06	98-05-02 14:06	–205	11	3	18	4	45	30	1418	720	5	24	12	16
18	00-09-18 00	00-09-16 05:18	–201	25	3	35	5	64	14	1493	2020	–4	0	12	–2
19[b]	04-07-27 14	04-07-25 14:54	–197	–21	–14	25	5	75	31	1289	1316	9	18	17	2
20	01-10-21 22	01-10-19 16:50	–187	9	0	17	1	43	25	1452	1544	–5	2	1	9
21	*00-10-05 14*	*NA*	*–182*												
22	*99-09-23 00*	*NA*	*–173*												
23	*98-09-27 10*	*no image*	*–155*												
24	98-11-08 07	98-11-05 20:44	–149	6	6	6	6	14	15	3568	2419	–19	–10	–7	–15
25	*04-07-25 12*	*NA*	*–148*												
26	*00-05-24 09*	*NA*	*–147*												
27	05-09-11 11	05-09-09 19:48	–147	–24	–8	–26	–11	67	28	1903	2492	–5	–5	19	–11
28[b]	06-12-15 08	06-12-13 02:54	–146	–36	–18	14	2	67	29	2170	1262	–5	22	13	–16
29	*03-05-30 00*	*NA*	*–144*												
30	05-05-30 14	05-05-26 15:06	–138	–11	1	16	–2	52	30	633	863	–7	–15	–18	8
31	*05-05-08 19*	*NA*	*–127*												
32	*05-01-18 09*	*multiple CMEs*	*–121*												
33	02-05-23 18	02-05-22 03:50	–109	–14	NA	21	NA	35	NA	1957	NA	4	NA	18	–3
34	*05-01-22 07*	*NA*	*–105*												
35	*05-01-08 03*	*NA*	*–096*												
36	*99-07-31 02*	*NA*	*–053*												

[a]Storm minimum D_{st} time is given in the format "year-month-day hour." CME start time means UT and the date (format "year-month-day hour:minute"), when the CME is first seen in LASCO C2 coronagraph image. "CME cone axis lat." means the CME cone axis latitude, derived using the cone model analytical and automatic methods. "CME cone axis lon." means the CME cone axis longitude derived using the cone model analytical and automatic methods. "CME cone radius" means the CME cone half opening angle, derived using the cone model analytical and automatic methods. "CME V_{rad}" means the initial CME radial speed in km/s, derived using analytical and automatic methods. "Shock arrival time error" means the difference in hours between CME shock arrival time predicted by the model and observed by the ACE satellite. WSA-ENLIL analytical method error, thirteenth column; WSA-ENLIL automatic method error, fourteenth column; reference model V_{ref} = 850 km/s error, fifteenth column; empirical model ESA error, sixteenth column. The error is negative if the observed shock arrival was later than model predicted and is positive in the opposite case. NA, not applicable. Italic font denotes cases where we did/could not run the model.

[b]Events studied previously by *Taktakishvili et al.* [2009].

parameters assuming that a CME propagates with nearly constant angular width in a radial direction and that the expansion is isotropic. Later *Xie et al.* [2004] developed an analytical method for determining the parameters of halo CME, angular width of the cone, propagation orientation and radial speed, using coronagraph images.

[12] Recently *Pulkkinen et al.* [2010] developed a novel method for the automatic determination of cone model parameters from coronagraph images. The method uses both standard image processing techniques to extract the CME extent from white light coronagraph images and a novel inversion routine providing the final cone parameters. A bootstrap technique is used to return a distribution of possible cone model parameter solutions. Importantly, this provides direct means for ensemble predictions of transient propagation in the heliosphere. An initial validation of the automatic method was carried out by *Pulkkinen et al.* [2010] by means of comparison to analytically determined cone model parameters using the method of *Xie et al.* [2004]. It was shown using 14 halo CME events that there

is reasonable agreement, especially between the heliocentric locations of the cones derived with the two methods.

[13] Hereafter, whenever we refer to "analytical," we mean CME parameters determined using the analytical method, and similarly "automatic" means that CME parameters were obtained using the automatic method.

[14] ENLIL is a time-dependent 3-D MHD model of the heliosphere [*Odstrcil and Pizzo*, 1999]. It solves equations for plasma mass, momentum and energy density, and magnetic field, using a Total-Variation-Diminishing Lax-Friedrichs algorithm. Its inner radial boundary is located beyond the critical point (where the solar wind flow becomes faster than fast MHD mode characteristic speed), typically at 21.5 R_s. ENLIL can accept boundary condition information from the Wang-Sheeley-Arge (WSA) coronal model [*Arge and Pizzo*, 2000] and MAS MHD model of solar corona [see, e.g., *Mikić et al.*, 1999]. In this paper we studied CME events using WSA-ENLIL model combination.

[15] WSA models the global magnetic field between the solar surface and a bounding spherical surface, where the magnetic field is assumed to be radial. The photospheric magnetic field is determined from synoptic magnetogram data. WSA computes the solar wind speed at the bounding surface using an empirical relationship. National Solar Observatory Kitt Peak magnetograms were used as input for the WSA model in this study. ENLIL applies this WSA output at its inner boundary and propagates the solar wind, including the CME, throughout the heliosphere.

[16] In the simulations presented here, ENLIL uses a uniformly spaced grid of size 256 × 30 × 90, where 256 is the number of grid points in radial direction (range from 21.5R_s to 2 AU), 30 is the number of grid points in latitude (perpendicular to the ecliptic plane, range from −60° to +60°), and 90 is the number of grid points in longitude (range from 0° to 360°. The temporal resolution (time step of the output) was approximately 7 minutes. Run execution time length of individual CME event with these parameters is approximately 2 h on a 4 processor machine, which is much faster than real time and is a very good characteristic for forecasting purposes.

4. Efficiency of the Cone Model Approach in CME Modeling

[17] Events listed in Table 1 are ranked (first column) by the measured minimum D_{st} index value (fourth column) of the geomagnetic storm caused by the corresponding CME event. The CME events studied previously by *Taktakishvili et al.* [2009] are ranked in this list as 2, 3, 5, 13, 19 and 28 and marked by b. The second column shows the start time and the date of the geomagnetic storm given in the format yy-mm-dd hh, the third column shows the corresponding CME start time (UT) from the LASCO catalog in the format yy-mm-dd hh:mm.

[18] Out of 36 strong geomagnetic storms listed in Table 1 we were able to analyze 20 corresponding CME events using the analytical method for the CME parameter determination and 19 events using the automatic method: in one case (rank 33) it was not possible to derive the CME parameters using the automatic method, because two different CMEs occurred simultaneously. In three cases (ranks 8,15,32) there were multiple CMEs and multiple storms closely separated in time, so that it was difficult to associate a particular geomagnetic storm to a particular CME. In two cases there were no images available in the CME catalog (ranks 16 and 23). In eleven cases it was impossible to derive CME parameters due to the nonhalo CME or poor image quality.

[19] Geomagnetic storm versus CME event association listed in Table 1, which we obtained independently, in all cases but one (rank 4) coincide with the events listed in the paper by *Zhang et al.* [2007].

5. Comparison of Cone Parameters Obtained Using Analytical and Automatic Methods

[20] The fifth and sixth columns in Table 1 display estimated CME cone axis latitude using analytical and automatic methods respectively. Here zero latitude corresponds to the ecliptic plane, positive latitude is measured toward the north, and negative is measured toward the south. Similarly the seventh and eighth columns show cone axis longitude obtained using the two methods. Here zero longitude corresponds to the Sun-Earth line, positive longitude direction corresponds to the counterclockwise rotation from the Earth location in the ecliptic plane, and negative corresponds to the clockwise rotation. The ninth and tenth columns display estimated cone half opening angles, called cone radii. Finally the eleventh and twelfth columns give the estimated initial radial speeds of the CMEs using the analytical and automatic methods respectively.

[21] In Figure 1 we plotted 4 diagrams of the values listed in the fifth through twelfth columns in Table 1. Figure 1a shows a diagram V_{auto} versus V_{analyt} for the estimated speeds, Figure 1b shows a diagram $\mathrm{lat}_{\mathrm{auto}}$ versus $\mathrm{lat}_{\mathrm{analyt}}$ for the estimated cone axis latitudes, Figure 1c demonstrates a $\mathrm{lon}_{\mathrm{auto}}$ versus $\mathrm{lon}_{\mathrm{analyt}}$ diagram for the estimated cone axis longitudes. Figure 1d shows the estimated cone radii for the two methods versus each other. As you can see the analytical method gives much larger cone radii than the automatic method. The reason for this discrepancy is most likely the fact that the values of cone radii estimated by the automatic method are concentrated around the climatological value of the cone radius rad = 30° used in the current version of this method. This value is an average of limb CME cone half opening angles observed over the large period of time [*Yashiro et al.*, 2004]. Recently *Gopalswamy et al.* [2009] and *Michalek et al.* [2009] demonstrated that this may not be the case for most of the fast CMEs. See more detailed discussion in the next Section.

[22] Thus, the two methods for the determination of CME cone parameters for the studied events give qualitatively consistent results for the CME speed and direction, although the results sometimes differ substantially.

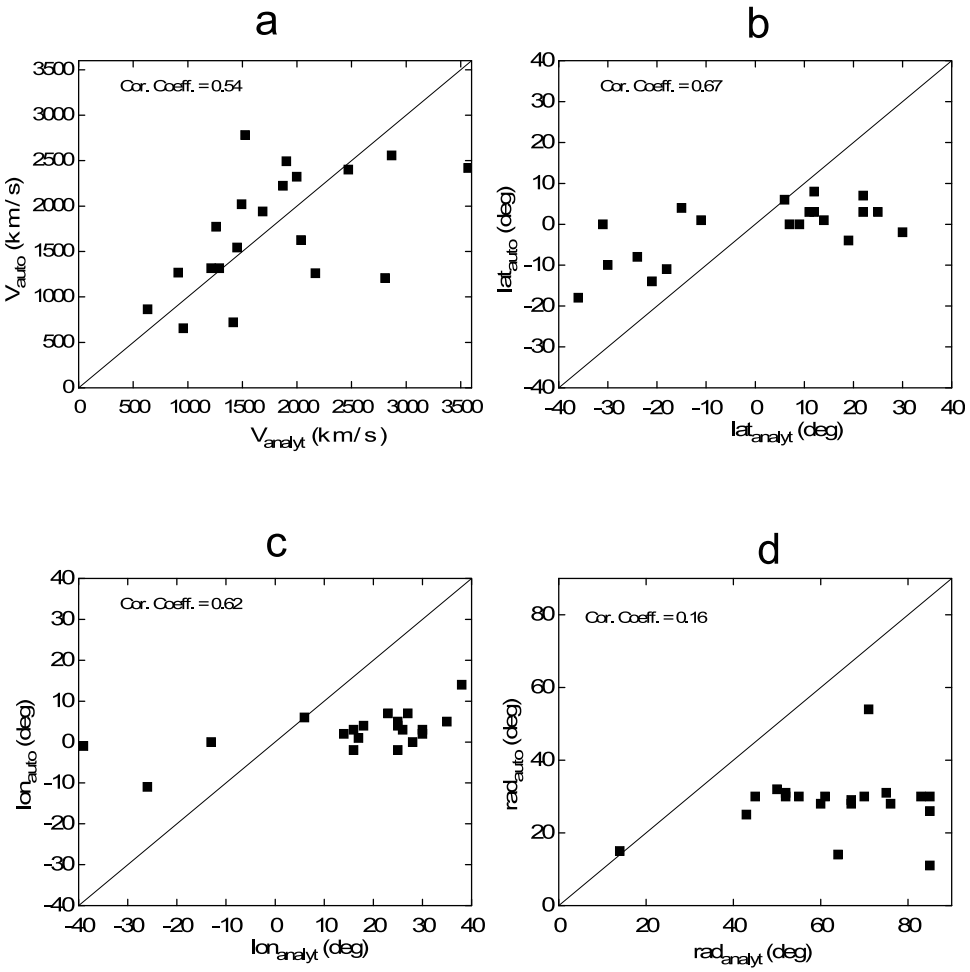

Figure 1. The parameters of CMEs listed in Table 1 derived from LASCO C3 images using analytical versus automatic methods. (a) V_{auto} versus V_{analyt} diagram of the estimated initial CME speeds (in km/s), (b) lat_{auto} versus lat_{analyt} diagram of the estimated cone axis latitudes (in degrees), (c) lon_{auto} versus lon_{analyt} diagram of the estimated cone axis longitudes (in degrees), and (d) rad_{auto} versus rad_{analyt} diagram of the estimated cone half opening angles/radiuses (in degrees).

The two methods give significantly different results for the cone opening angles.

6. Simulation Results: Shock Arrival Time

[23] We compared the CME shock arrival times predicted by our ENLIL cone model simulations to the observed shock arrival times. The prediction error,

$$\Delta t_{err} = t^{arr}_{enlil} - t^{arr}_{obs} \quad (1)$$

rounded to the nearest of 0.5 h, for each of the events are listed in the thirteenth and fourteenth columns of Table 1 for analytical and automatic methods respectively. The error is negative when ENLIL predicted a shock arrival time earlier than the observed shock arrival time, and is positive for late ENLIL prediction.

[24] In Figure 2 we plotted the arrival time errors versus event rank (model/analytical, blue squares; model/automatic, red squares).

[25] To evaluate the ENLIL cone model performance for the shock arrival times, it is useful to compare the simulation results to the results of reference models. The simplest reference model is propagation of the CME shock with some constant velocity. Taking the mean of initial plane of sky projection velocities for approximately 320 halo CMEs listed in the SOHO/LASCO catalog (http://cdaw.gsfc.nasa.gov/CME_list/) for the period of years 1996–2007, we obtained V_{ref} = 850 km/s. The corresponding transit time from the Sun to the ACE position is approximately 48 h. The arrival time errors for this reference model are listed in the fifteenth column of Table 1 and plotted in Figure 2 (white squares).

[26] We also compared the ENLIL cone model results to the results of the empirical shock arrival model (ESA) of

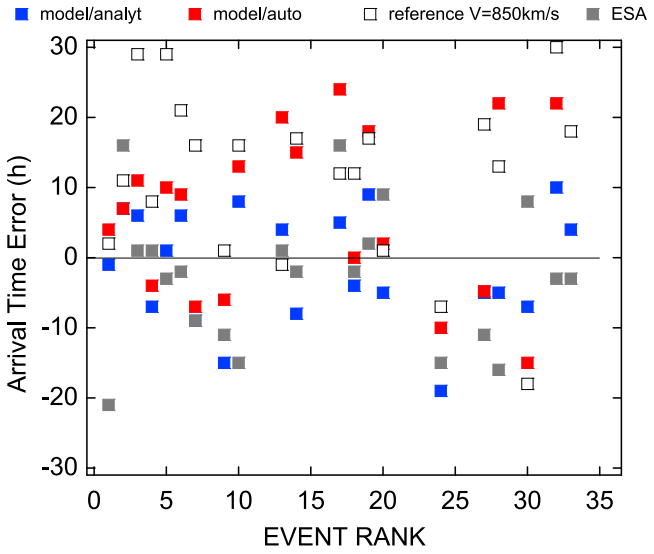

Figure 2. Arrival time errors (in hours) for the CME events listed in Table 1 versus event rank. WSA-ENLIL analytical method, blue squares; WSA-ENLIL automatic method, red squares; reference model V_{ref} = 850 km/s, white squares; and empirical model ESA, grey squares.

Gopalswamy et al. [2005]. We used calculated plane of sky velocities given in SOHO/LASCO catalog as input to the empirical Equation (11) from *Xie et al.* [2006] to calculate the shock transit times for the cases we analyze in this paper. The resulting values of the arrival time errors are given in the sixteenth column of Table 1 and plotted in Figure 2 (grey squares).

[27] WSA-ENLIL analytical cone model combination has tendency toward early arrival prediction for the modeled set of events. The mean error is –1.2 h, the largest early arrival prediction error for this combination is –19 h, the largest late arrival prediction error is 9 h. This similar result was obtained in our previous study *Taktakishvili et al.* [2009]. This could be mainly the result of overestimation of CME material density, i.e., its mass, by ENLIL model for the default free parameters'set used throughout this study, since more massive CMEs experience less slowing down during their propagation in the heliosphere. See more detailed discussion on the modeled density issue in the next Section.

[28] On the contrary, WSA-ENLIL automatic cone model combination has tendency toward late predictions for the modeled set of events. The mean error for this combination is 6.5 h, the largest late arrival prediction error is 24 h, the largest early arrival prediction error is –15 h. The derived CME speeds for both analytical and automatic methods are not very different from each other, so the reason for this discrepancy is probably the underestimation of the CME cone opening angle/CME radius, i.e., CME mass, by the current version of the automatic method (see above). As it has been already mentioned in the previous Section, in the current version of the WSA-ENLIL automatic combination we used the climatological value of rad = 30° for the cone half opening angle, which may not be true for the fast CMEs that we considered in this paper. Recent studies by *Gopalswamy et al.* [2009] and *Michalek et al.* [2009] demonstrated that for fast CMEs (speed ≥ 800 km/s, the cone radius is usually much larger than 30° and is in most cases proportional to the CME speed. It is shown that statistically CME radius grows with the CME initial speed. We are currently working on a new version of the automatic method utilizing more modern optimization routines (stochastic tunneling). We will also include the results of studies by *Gopalswamy et al.* [2009] and *Michalek et al.* [2009] in this new version. It can be expected that the modifications will improve the automatic cone model determination results.

[29] The reference model has very strong tendency toward late predictions for the modeled set of events: the average error is approximately 11.7 h. The average error of the ESA model for the modeled cases was –2.8 h, indicating a tendency toward earlier than observed arrival times.

[30] The mean of the absolute error $|\Delta t_{err}|$ for the WSA-ENLIL analytical method is 6.9 h with the standard deviation of 4.2 h. For WSA-ENLIL automatic method the mean of the absolute error is 11.2 h (standard deviation 7.2h). For the reference model V_{ref} = 850 km/s and ESA the mean of the absolute error is respectively 14.2 h (standard deviation 8.9) and 8.0h (standard deviation 6.5).

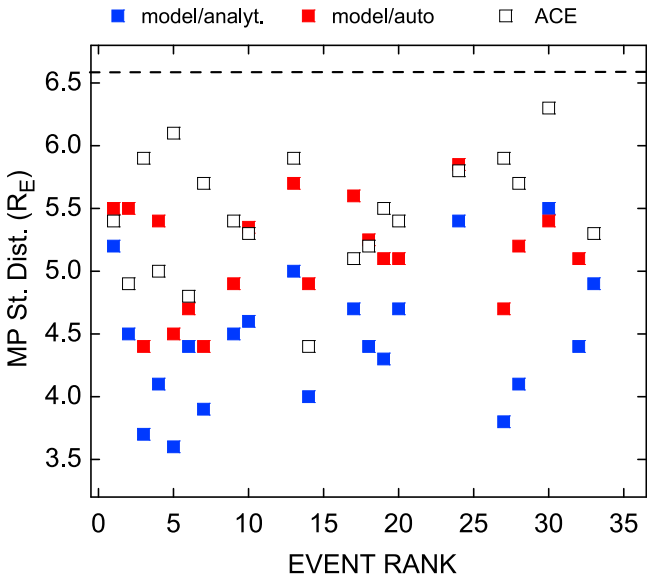

Figure 3. Estimated magnetopause standoff distances (in R_E) for the CME events listed in Table 1 versus event rank. WSA-ENLIL analytical method, blue squares; WSA-ENLIL automatic method, red squares; derived from ACE observations, white squares. The dashed line corresponds to the geosynchronous orbit of 6.6 R_E.

[31] As we can see WSA-ENLIL analytical cone model combination on the average does better job than the reference and slightly better than the empirical model, while current WSA-ENLIL automatic combination beats the reference model but does slightly worse than the empirical model.

7. Magnitude of Impact: Estimation of the Magnetopause Standoff Distance

[32] Another parameter that is very important for the space weather forecasters and operators, besides CME arrival time, is the magnitude of the impact of the CME on the magnetosphere. We measure this parameter by the degree of the deformation of the Earth's magnetosphere due to the interaction with the CME. The physical quantity mostly responsible for the strength of the impact of the CME on the magnetosphere is the dynamic pressure of the solar wind. In our previous study [*Taktakishvili et al.*, 2009] we estimated the magnetic field strength required to "stop" the solar wind stream for a modeled CME event using the equation given by *Spreiter et al.* [1965] for the balance of dynamic and magnetic field pressures at the magnetopause. Assuming that the magnetic field close to the Earth is a dipole, we can then estimate the magnetopause standoff distance for different CME events [see *Taktakishvili et al.*, 2009].

[33] In Table 2 we present the minimum magnetopause standoff distances given by the model calculations using analytical (fourteenth column), automatic (fifteenth column) methods for determination of the CME parameters and observations (sixteenth column), estimated by using actual ACE measurements of the solar wind speed and density (event rank is given in the first column). In Figure 3 we plot the same data versus event rank. Blue squares correspond to the WSA-ENLIL analytical model results, red squares, WSA-ENLIL automatic; white squares, ACE measurements. The horizontal dashed line represents the geosynchronous orbit distance $R_{gs} = 6.6R_e$.

[34] Anticipating magnetopause standoff distance at or inside R_{gs} is especially important for the satellite operators for various reasons, such as that penetration of the solar wind plasma beyond the geosynchronous orbit and consequent exposure of a satellite to it can impact control systems. We see that both the WSA-ENLIL analytical and WSA-ENLIL automatic model combinations overestimate the deformation of the magnetopause for almost all of the events we modeled.

[35] In the sixteenth column of Table 2, next to the numeric value, there is a sign indicating association with actual geosynchronous magnetopause crossings (GMC) for each of the events, "Y" meaning that GMC actually happened for that particular event, "N" that GMC did not take place and question mark meaning that it was not clear from the data that GMC took place or not. For the majority of the studied events there was a crossing of the geosynchronous orbit by the magnetopause caused by CME impact.

[36] In almost all the cases WSA-ENLIL automatic combination gives better result for the minimum magnetopause standoff distance, closer to ACE observations. The mean of the obtained magnetopause standoff distances for modeled events using analytical and automatic methods are $4.6R_e$ and $5.1R_e$ respectively. The mean of the standoff distances for the same events based on the ACE data is $5.4R_e$. We should also remember, that the lower limits of the estimated standoff distances are shown in Figure 3, and these values correspond to the instantaneous peaks of the CME disturbance at the magnetopause that probably will not be sustained for long period of time.

[37] Table 2, the second through tenth columns, and Figures 4 and 5 help to understand better the reason for overestimation of CME impact predicted by the model. In Figure 4a is plotted time dependence of the solar wind density (top panel), magnetic field (middle panel) and speed (bottom panel) at the ACE satellite location given by the model (WSA-ENLIL analytical, blue line; WSA-ENLIL automatic, red line) and ACE observations (black line) for a 2 day time window around the shock arrival time for the event ranked 20. Figure 4a demonstrates that the density peak is overestimated approximately 3 times, the magnetic field is underestimated ~2.5 times (see the detailed discussion on the modeled magnetic field strength in the next Section), while the speed is not too far from the observed value for this particular event. Figures 5a, 5b and 5c statistically confirm this result. In this plots we display peak values at the shock for the density (5a), magnetic field (5b) and speed (5c) respectively given by the both methods of the CME parameter determination, versus ACE observations for all of the studied events. The same data is listed in the second through tenth columns of Table 2.

[38] So, clearly the reason of the discrepancy with the observations is overestimation by the model of the solar wind density at the CME shock arrival. The current ENLIL version assumes a spherical homogeneous cloud launched in the heliosphere which gives a large momentum (dynamic pressure). The discrepancy between the model and observations should be smaller in the upcoming version of ENLIL with more realistic flux-rope-like structure of CMEs, for example taking into account cavity in the CME cloud. Another reason can be the uncertainty in a free parameter, such as e.g. initial ratio between the CME material density and the ambient fast solar wind density. To understand why the ENLIL cone model runs overestimates the impact in the work by *Taktakishvili* et al. [2010] we also performed simulations varying this free parameter. The results demonstrated that the initial density ratio can be important for the estimation of the impact, as well as the CME arrival time.

8. Estimation of the Convective Electric Field Induced by the CME

[39] The solar wind convective electric field defined here as $E_{sw} = -v \cdot B_z$, where v is the bulk solar wind speed and B_z is the z component of the solar wind magnetic field **B** in

Table 2. Modeling and Observational Results for the Events Listed in Table 1[a]

	Max Density at the Shock (cm^{-3})			Max. Mag. Field Magnitude at the Shock (nT)			Max. Solar Wind Speed at the Shock (km/s)			Induced Electric Field (mV/m)			MP Standoff Distance (Re)		
Rank	Analyt.	Auto	ACE	Analyt.	Auto	ACE	Analyt.	Auto	ACE	Analyt.	Auto	ACE	Analyt.	Auto	ACE[b]
01	32	29	18	6	5	56	662	582	703	3.4	3.0	34.3	5.2	5.5	5.4 (Y)
02[c]	56	22	30	13	8	47	735	649	716	11.5	5.1	32.1	4.5	5.5	4.9 (Y)
03[c]	85	50	NA	23	16	38	1076	826	NA	24.4	13.3	32.6	3.7	4.4	NA (Y)
04	56	22	65	10	11	46	949	699	648	10.6	7.6	31.8	4.1	5.4	5.0 (Y)
05[c]	69	56	NA	14	15	30	1279	749	NA	17.8	11.0	42.4	3.6	4.5	NA (Y)
06	60	52	20	15	13	34	778	680	1010	12.1	9.1	54.2	4.4	4.7	4.8 (Y)
07	51	31	42	16	13	45	1229	1054	729	19.5	13.8	8.9	3.9	4.4	5.7 (N)
08	–	–	–	–	–	–	–	–	–	–	–	–	–	–	–
09	53	53	30	9	10	24	740	598	625	6.5	6.0	17.8	4.5	4.9	5.4 (Y)
10	51	33	25	8	7	35	733	601	732	5.7	4.1	25.0	4.6	5.3	5.3 (Y)
11	–	–	–	–	–	–	–	–	–	–	–	–	–	–	–
12	–	–	–	–	–	–	–	–	–	–	–	–	–	–	–
13[c]	49	39	15	9	8	21	575	447	639	5.4	3.4	20.6	5.0	5.7	5.9 (N)
14	51	47	43	13	9	37	1093	616	948	11.0	5.7	49.8	4.0	4.9	4.4 (Y)
15	–	–	–	–	–	–	–	–	–	–	–	–	–	–	–
16	–	–	–	–	–	–	–	–	–	–	–	–	–	–	–
17	63	33	23	16	9	39	631	500	833	10.1	4.2	32.4	4.7	5.6	5.1 (?)
18	46	28	33	13	12	30	888	704	695	11.4	8.3	20.6	4.4	5.2	5.2 (Y)
19[c]	96	61	9	16	13	19	667	506	1002	10.4	6.5	26.8	4.3	5.1	5.5 (Y)
20	69	56	17	12	12	25	589	517	649	7.0	6.0	17.6	4.7	5.1	5.4 (Y)
21	–	–	–	–	–	–	–	–	–	–	–	–	–	–	–
22	–	–	–	–	–	–	–	–	–	–	–	–	–	–	–
23	–	–	–	–	–	–	–	–	–	–	–	–	–	–	–
24	26	24	21	7	6	35	626	539	639	4.7	3.0	22.1	5.4	5.8	5.8 (N)
25	–	–	–	–	–	–	–	–	–	–	–	–	–	–	–
26	–	–	–	–	–	–	–	–	–	–	–	–	–	–	–
27	48	20	NA	18	13	18	1297	1051	1045	22.9	13.9	18.3	3.8	4.7	5.9 (N)
28[c]	74	56	9	11	9	15	832	492	890	8.8	4.2	15.1	4.2	5.2	5.7 (Y)
29	–	–	–	–	–	–	–	–	–	–	–	–	–	–	–
30	28	25	17	8	9	19	586	641	501	5.0	5.9	10.6	5.5	5.4	6.3 (?)
31	–	–	–	–	–	–	–	–	–	–	–	–	–	–	–
32	–	–	–	–	–	–	–	–	–	–	–	–	–	–	–
33	41	*NA*	15	9	*NA*	38	679	*NA*	871	7.5	*NA*	29.4	4.9	*NA*	5.3 (Y)
34	–	–	–	–	–	–	–	–	–	–	–	–	–	–	–
35	–	–	–	–	–	–	–	–	–	–	–	–	–	–	–
36	–	–	–	–	–	–	–	–	–	–	–	–	–	–	–

[a]"Max density at the shock" means peaked values for the solar wind density given by the WSA-ENLIL analytical and automatic cone model combinations and ACE observations. "Max mag. field magnitude at the shock" means peaked values for the solar wind magnetic field magnitude given by the WSA-ENLIL analytical and automatic cone model combinations and ACE observations. "Max solar wind speed at the shock" means peaked values for the solar wind speed given by the WSA-ENLIL analytical and automatic cone model combinations and ACE observations. "Induced electric field" means estimated induced electric field in mV/m using WSA-ENLIL analytical cone model method, WSA-ENLIL automatic, and induced electric field corresponding to ACE observations. "MP standoff distance" means estimated magnetopause standoff distances in Earth radii R_E: WSA-ENLIL analytical, WSA-ENLIL automatic, and standoff distance corresponding to ACE observations. NA, not applicable. Italic font denotes cases where we did/could not run the model.

[b]"Y" indicates that GMC actually happened for the event, "N" indicates that GMC did not take place, and a question mark means that it was not clear from the data if GMC took place or not.

[c]Events studied previously by *Taktakishvili et al.* [2009].

GSM coordinates, is an important parameter quantifying the strength of the solar wind driving of the magnetospheric activity. *Pulkkinen et al.* [2008, 2009] used convective electric field predictions generated by WSA-ENLIL cone model approach to couple CME and solar wind bulk plasma and magnetic field parameters to geomagnetic field fluctuations on the surface of the Earth. They estimated geomagnetically induced current (GIC) levels at high-latitude locations. Accurate predictions of (maximum over events) E_{sw} help to forecast GIC impact on technological systems on the ground. In discussion below, the maximum value of E_{sw} taken over individual events is used.

[40] In Table 2, the eleventh, twelfth and thirteenth columns are listed maximum convective electric field values provided by model using automatic and analytic methods for CME parameter determination as well as the maximum values corresponding to ACE observations. Figure 5d shows the these values plotted versus event rank. Both modeling approaches underestimate the maximum convective electric fields by a factor of ~2–3, on average, whereas for the strongest storm ranked 1 this factor is

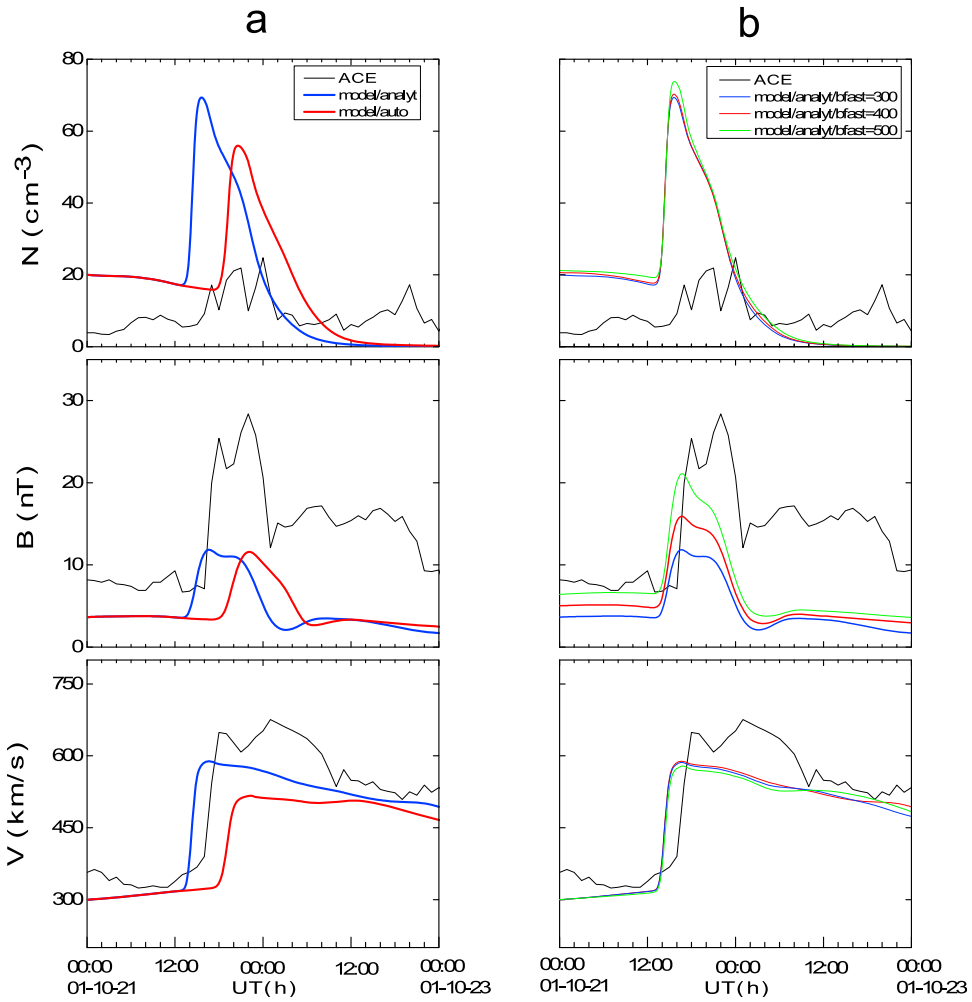

Figure 4. (a and b) Time series of solar wind parameters within a 2 day time window around CME shock arrival for the event ranked 20 in Table 1. Both top panels in Figures 4a and 4b show solar wind density (cm^{-3}), middle panels show magnetic field magnitude (nT), and bottom panels show speed (km/s). Figure 4a demonstrates solar wind parameters given by WSA-ENLIL analytical (blue line) and WSA-ENLIL automatic (red line) cone model combinations and corresponding ACE observations (black line) for the fixed default values of the ENLIL free parameters. Figure 4b shows solar wind parameters given by WSA-ENLIL analytical cone model combination for the different values of the magnetic field scaling free parameter *bfast*: 300 (default value), blue line; 400, red line; 500, green line; ACE observations, black line.

unusually high ~10. This result is in agreement with *Pulkkinen et al.* [2009], who indicated that WSA-ENLIL model's incapability to generate the extreme E_{sw} is due to lack of realistic internal magnetic field structure within simulated CMEs.

[41] The underestimation of the convective electric field is obviously due to underestimation of the shock magnetic field for almost all of the events studied in this paper, illustrated by the results shown for one of the events in Figure 4a (middle panel) and all events shown in Figure 5c (see discussion in the previous Section). It is essential to note here that in this study we used WSA-ENLIL model combination in so-called "forecasting" mode: the default values of the ENLIL free parameters resulted from previous calibration studies were kept constant throughout the studied events. These free parameters are used by ENLIL to process the WSA data in order to provide typical values observed at L1 point and ensure robustness of the model run. ENLIL computes CME shock compression rate and field draping, which are the factors of the background magnetic field strength. However, calibration of the magnetic field magnitude varies depending on solar cycle, solar observatory instrumentation and postprocessing method of photospheric field observations. So, in "research" mode, when the model is used for example to reconstruct a par-

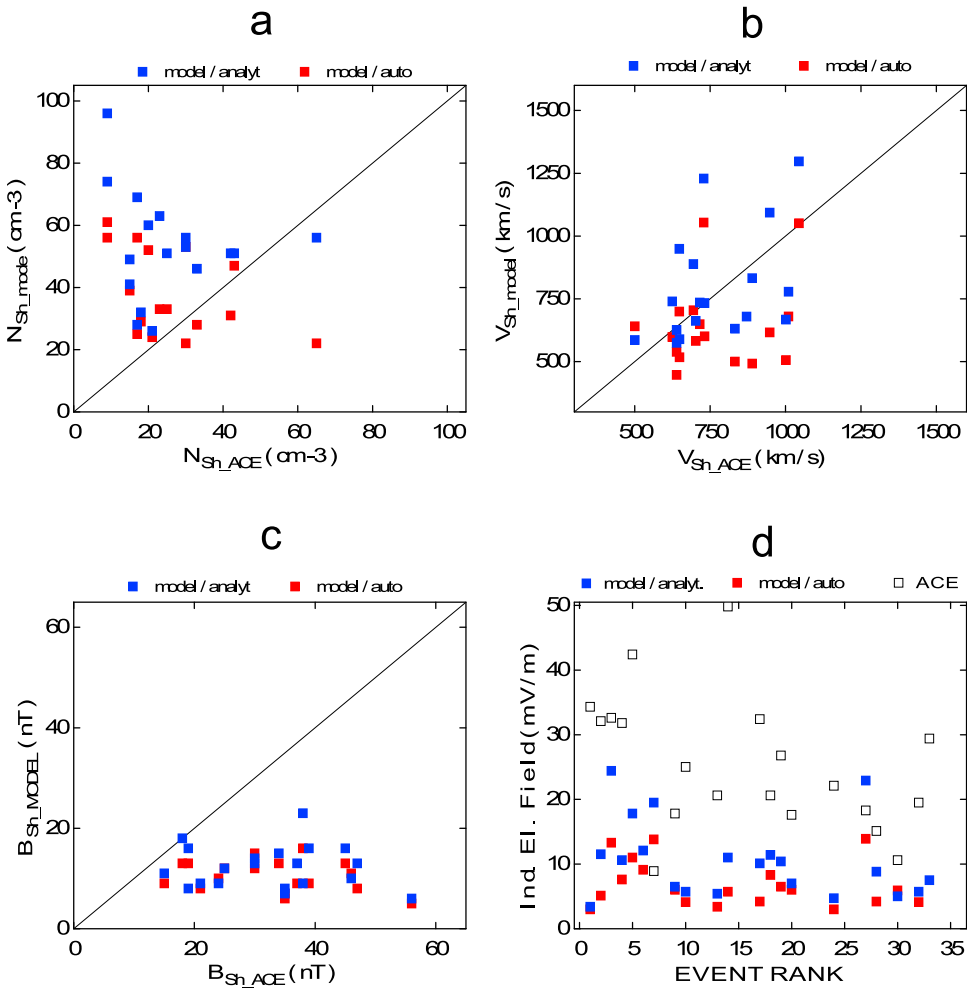

Figure 5. (a, b, and c) Peak values of the solar wind parameters at the CME shock arrival time given by the WSA-ENLIL analytical and WSA-ENLIL automatic cone model combinations versus corresponding peak values observed by the ACE satellite and (d) estimated induced electric field for the events listed in Table 1. Blue squares correspond to WSA-ENLIL analytical cone model combination, red squares correspond to WSA-ENLIL analytical cone model combination, and white squares correspond to ACE observations. Figure 5a shows N_{Sh_model} versus N_{Sh_ACE} diagram of the density (cm^{-3}), Figure 5b shows V_{Sh_model} versus V_{Sh_ACE} diagram for the speed (km/s), and Figure 5c shows B_{Sh_model} versus B_{Sh_ACE} diagram for the magnetic field magnitude (nT). Figure 5d shows induced electric field estimated by the model (blue squares, analytical method; red squares, automatic method) and corresponding to ACE measurements (white squares) versus event rank.

ticular event, the magnetic field has to be adjusted to provide better match with specific observations.

[42] In Figure 4b we illustrate the dependence of the model predicted solar wind parameters at the ACE location on a free magnetic field scaling parameter *bfast* used in ENLIL model, for the event ranked 20. The detailed explanation of this free parameter and a possibility to study how varying of *bfast* modifies modeling results will be available through the coming new version of the ENLIL model at the Runs on Request system of the Community Coordinated Modeling Center (CCMC, http://ccmc.gsfc.nasa.gov).

[43] The top panel in Figure 4b shows solar particle number density, the middle panel shows magnetic field strength, and the bottom panel shows solar wind speed. ACE observations are presented by solid black line and the parameters for *bfast* = 300 (default value), 400 and 500 are presented with blue, red and green lines respectively. Note that increasing of *bfast* brings magnetic field strength peak closer to the observed value, while the shock compression rate is almost the same. At the same time the overall solution for the CME shock arrival, density and speed is practically unchanged. Therefore, it is important to conclude that the results for the shock arrival time and

magnetopause standoff distances presented in this study, where the goal was to explore WSA-ENLIL performance in the forecasting mode, will not be influenced by this free parameter.

[44] On the other hand, accurate estimate of the induced electric field requires case to case adjusting of *bfast*. Clearly the same adjustment is needed also for some other space weather applications where the magnetic field value is important, e.g. for using of the heliospheric parameters as input to solar energetic particle (SEP) models, or magnetospheric studies.

9. Summary

[45] We studied the performance of the WSA-ENLIL cone model in modeling the propagation of the strongly geoeffective CMEs in the heliosphere. The approach used in this study is addressing space weather forecasting and operational needs. In contrast to *Taktakishvili et al.* [2009], where we started the analysis by looking for clear CME signatures in the white light coronagraph data and then proceeded to model the interplanetary consequences at 1 AU, in this study we started by generating a list of observed geomagnetic storm events and then worked our way back to remote solar observations and carried out the corresponding CME modeling.

[46] OMNI data set for D_{st} and K_p indices for the period of January 1996 to February 2009, which reflects the SOHO/LASCO CME data catalog availability, was analyzed. We identified 36 individual strong geomagnetic storm events ($K_p \geq 8$), then ranked them as a function of the minimum D_{st} index taken over the event.

[47] Cone model initial CME parameters, speed, cone axis direction and opening angle, were obtained from the SOHO/LASCO CME catalog imagery, using analytical and automatic methods. The two methods give qualitatively similar results for the CME speed and direction, but for the opening angle results differ significantly.

[48] Out of 36 particularly strong geomagnetic storms we were able to analyze 20/19 of associated CME events using analytical/automatic method of the CME parameter determination for the WSA-ENLIL cone model approach. In the rest of the cases there were either multiple CMEs and multiple storms closely separated in time, so that it was difficult to associate particular geomagnetic storm to particular CMEs, or there were no images available in the CME catalog, or as in a majority of cases, it was impossible to derive CME parameters due to the non halo CME or poor image quality.

[49] We compared the results of the WSA-ENLIL/cone model simulation with the ACE satellite observations and the results of a simple reference model and empirical shock arrival model of *Gopalswamy et al.* [2005].

[50] We focused on three important parameters: the arrival time of the CME shock, the magnitude of the CME impact on the magnetosphere, characterized by the minimum magnetopause standoff distance corresponding to the CME dynamic pressure and convective electric field magnitude induced by the CME.

[51] In this set of modeled events for the WSA-ENLIL analytical method combination there are more earlier arrival predictions than late arrival predictions with mean absolute error of 6.9 h for the total set. In contrast to that for WSA-ENLIL automatic method combination there are more later arrival predictions than earlier arrival predictions. The mean absolute error of 11.2 h for the total set. Both approaches for the CME parameter determination do better job than the simple reference model (mean absolute error 14.3 h). Empirical model on the average (mean absolute error 8.0 h) demonstrates smaller errors than WSA-ENLIL automatic method combination.

[52] For the magnetopause standoff distance prediction both modeling approaches overestimate the deformation of the magnetopause for almost all of the events we modeled. The reason for that is overestimation by the model of the solar wind density at the CME shock arrival. Both modeling approaches underestimate the maximum convective electric fields induced by the CME. This is most likely due to lack of realistic internal magnetic field structure within simulated CMEs.

[53] The modeling results are expected to improve in the upcoming version of ENLIL with more realistic flux-rope-like structure of CMEs.

[54] **Acknowledgments.** We thank L. Rastaetter, M.-C. Fok, and S.-H. Chen for useful discussions. All simulations carried out at this work were done at the Community Coordinated Modeling Center at NASA Goddard Space Flight Center. We used OMNI (http://omniweb.gsfc.nasa.gov/) and SOHO/LASCO catalog (http://cdaw.gsfc.nasa.gov/CME_list) date for our analysis.

References

Anderson, C. W., III, L. J. Lanzerotti, and C. G. MacLennan (1974), Outage of the L4 system and the geomagnetic disturbances of 4 August 1972, *Bell Syst. Technical J., 53*, 1817–1837.

Arge, C. N., and V. P. Pizzo (2000), Improvement in the prediction of solar wind conditions using near-real time solar magnetic field updates, *J. Geophys. Res., 105*, 10,465–10,479.

Berdichevsky, D. B., A. Szabo, R. P. Lepping, and A. F. Vinas (2000), Interplanetary fast shocks and associated drivers observed through the 23rd solar minimum by Wind over its first 2.5 years, *J. Geophys. Res., 105*, 27,289–27,314.

Dryer, M., Z. Smith, C. D. Fry, W. Sun, C. S. Deehr, and S.-I. Akasofu (2004), Real-time shock arrival predictions during the "Halloween 2003 epoch," *Space Weather, 2*, S09001, doi:10.1029/2004SW000087.

Fry, C. D., M. Dryer, Z. Smith, W. Sun, C. S. Deehr, and S.-I. Akasofu (2003), Forecasting solar wind structures and shock arrival times using an ensemble of models, *J. Geophys. Res., 108*(A2), 1070, doi:10.1029/2002JA009474.

Gopalswamy, N., A. Lara, S. Yashiro, M. Kaiser, and R. Howard (2001), Predicting the 1-AU arrival times of coronal mass ejections, *J. Geophys. Res., 106*, 29,207–29,217.

Gopalswamy, N., A. Lara, P. K. Manoharan, and R. Howard (2005), An empirical model to predict the 1-AU arrival of interplanetary shocks, *Adv. Space Res., 36*, 2289–2294.

Gopalswamy, N., A. Dal Lago, S. Yashiro, and S. Akiyama (2009), The expansion and radial speeds of coronal mass ejections, *Cent. Eur. Astrophys. Bull., 33*, 115–124.

Gosling, J. T. (1993), The solar flare myth, *J. Geophys. Res., 98*, 18,937–18,949.

Kataoka, R., T. Ebisuzaki, K. Kusano, D. Shiota, S. Inoue, T. T. Yamamoto, and M. Tokumaru (2009), Three-dimensional MHD modeling of the solar wind structures associated with 13 December 2006 coronal mass ejection, *J. Geophys. Res.*, *114*, A10102, doi:10.1029/2009JA014167.

Kim, K.-H, Y.-J. Moon, and K.-S. Cho (2007), Prediction of the 1-AU arrival times of CME-associated interplanetary shocks: Evaluation of an empirical interplanetary shock propagation model, *J. Geophys. Res.*, *112*, A05104, doi:10.1029/2006JA011904.

Lugaz, N., W. B. Manchester IV, I. I. Roussev, G. Tóth, and T. I. Gombosi (2007), Numerical investigation of the homologous coronal mass ejection events from active region 9236, *Astrophys. J.*, *659*, 788–800.

McKenna-Lawlor, S. M. P., M. Dryer, M. D. Kartalev, Z. Smith, C. D. Fry, W. Sun, C. S. Deehr, K. Kecskemety, and K. Kudela (2006), Near real-time predictions of the arrival at Earth of flare-related shocks during Solar Cycle 23, *J. Geophys. Res.*, *111*, A11103, doi:10.1029/2005JA011162.

Michalek, G., N. Gopalswamy, and S. Yashiro (2009), Expansion speed of coronal mass ejections, *Sol. Phys.*, *260*, 401–406.

Mikić, Z., J. A. Linker, D. Schnack, R. Lionello, and A. Tarditi (1999), Magnetohydrodynamic modeling of the global solar corona, *Phys. Plasmas*, *6*, 2217–2224, doi:10.1063/1.873474.

Odstrcil, D., and V. J. Pizzo (1999), Distortion of the interplanetary magnetic field by three-dimensional propagation of coronal mass ejections in a structured solar wind, *J. Geophys. Res.*, *104*, 28,225–28,239, doi:10.1029/1999JA900319.

Odstrcil, D., P. Riley, and X. P. Zhao (2004), Numerical simulation of the 12 May 1997 interplanetary CME event, *J. Geophys. Res.*, *109*, A02116, doi:10.1029/2003JA010135.

Odstrcil, D., V. J. Pizzo, and C. N. Arge (2005), Propagation of the 12 May 1997 interplanetary coronal mass ejection in evolving solar wind structures, *J. Geophys. Res.*, *110*, A02106, doi:10.1029/2004JA010745.

Oler, C. (2004), Prediction performance of space weather forecast centers following the extreme events of October and November 2003, *Space Weather*, *2*, S08001, doi:10.1029/2004SW000076.

Pulkkinen, A., R. Pirjola, and A. Viljanen (2008), Statistics of extreme geomagnetically induced current events, *Space Weather*, *6*, S07001, doi:10.1029/2008SW000388.

Pulkkinen, A., A. Taktakishvili, D. Odstrcil, and W. Jacobs (2009), Novel approach to geomagnetically induced current forecasts based on remote solar observations, *Space Weather*, *7*, S08005, doi:10.1029/2008SW000447.

Pulkkinen, A., T. Oates, and A. Taktakishvili (2010), Automatic determination of the conic coronal mass ejection model parameters, *Sol. Phys.*, *261*, 115–126, doi:10.1007/s11207-009-9473-z.

Smith, Z., T. R. Detman, M. Dryer, and C. D. Fry (2005), Determining shock velocity inputs for Sun-to-Earth models, in *"Connecting Sun and Heliosphere": Proceedings of Solar Wind 11/SOHO 16*, edited by B. Fleck and T. H. Zurbuchen, *Eur. Space Agency Spec. Publ., ESA SP-592*, 771–774.

Spreiter, J. R., A. L. Summers, and A. Y. Alksne (1965), Hydromagnetic flow around the magnetosphere, *Planet. Space Sci.*, *14*, 223–253.

Taktakishvili, A., M. Kuznetsova, P. MacNeice, M. Hesse, L. Rastätter, A. Pulkkinen, A. Chulaki, and D. Odstrcil (2009), Validation of the coronal mass ejection predictions at the Earth orbit estimated by ENLIL heliosphere cone model, *Space Weather*, *7*, S03004, doi:10.1029/2008SW000448.

Taktakishvili, A., P. MacNeice, and D. Odstrcil (2010), Model uncertainties in predictions of arrival of coronal mass ejections at Earth orbit, *Space Weather*, *8*, S06007, doi:10.1029/2009SW000543.

Tóth, G., D. L. De Zeeuw, T. I. Gombosi, W. B. Manchester, A. J. Ridley, I. V. Sokolov, and I. I. Roussev (2007), Sun-to-thermosphere simulation of the 28–30 October 2003 storm with the Space Weather Modeling Framework, *Space Weather*, *5*, S06003, doi:10.1029/2006SW000272.

Wu, C.-C., C. D. Fry, S. T. Wu, M. Dryer, and K. Liou (2007), Three-dimensional global simulation of interplanetary coronal mass ejection propagation from the Sun to the heliosphere: Solar event of 12 May 1997, *J. Geophys. Res.*, *112*, A09104, doi:10.1029/2006JA012211.

Xie, H., L. Ofman, and G. Lawrence (2004), Cone model for halo CMEs: Application to space weather forecasting, *J. Geophys. Res.*, *109*, A03109, doi:10.1029/2003JA010226.

Xie, H., L. Gopalswamy, L. Ofman, O. C. St. Cyr, G. Michalek, A. Lara, and S. Yashiro (2006), Improved input to the empirical coronal mass ejection (CME) driven shock arrival model from CME cone models, *Space Weather*, *4*, S10002, doi:10.1029/2006SW000227.

Yashiro, S., N. Gopalswamy, G. Michalek, O. C. St. Cyr, S. P. Plunkett, N. B. Rich, and R. A. Howard (2004), A catalog of white light coronal mass ejections observed by the SOHO spacecraft, *J. Geophys. Res.*, *109*, A07105, doi:10.1029/2003JA010282.

Zhang, J., et al. (2007), Solar and interplanatery sources of major geomagnetic storms $Dst \leq -100$ nT) during 1996–2005, *J. Geophys. Res.*, *112*, A10102, doi:10.1029/2007JA012321.

Zhao, X. P., S. P. Plunkett, and W. Liu (2002), Determination of geometrical and kinematical properties of halo coronal mass ejections using the cone model, *J. Geophys. Res.*, *107*(A8), 1223, doi:10.1029/2001JA009143.

M. Hesse, M. Kuznetsova, P. MacNeice, and A. Taktakishvili, NASA Goddard Space Flight Center, Greenbelt, MD 20771, USA. (aleksandre.taktakishvili-1@nasa.gov)

D. Odstrcil, Department of Computational and Data Sciences, George Mason University, Fairfax, VA 22030, USA.

A. Pulkkinen, Institute of Astrophysics and Computational Physics, Catholic University of America, 620 Michigan Ave. NE, Washington, DC 20064, USA.